Bioactive Materials 6 (2021) 589–601

Contents lists available at ScienceDirect

Bioactive Materials

journal homepage: http://www.keaipublishing.com/biomat

Elastin-like polypeptide modified silk fibroin porous scaffold promotes osteochondral repair

Zhuoyue Chen[a], Qiang Zhang[b], Hongmin Li[a], Qi Wei[a], Xin Zhao[b,*], Fulin Chen[a,**]

[a] Provincial Key Laboratory of Biotechnology of Shaanxi, Key Laboratory of Resource Biology and Modern Biotechnology in Western China, Faculty of Life Science, Northwest University, 229 North TaiBai Road, Xi'an, Shaanxi Province, 710069, China
[b] Department of Biomedical Engineering, The Hong Kong Polytechnic University, Hung Hom, Hong Kong, China

ARTICLE INFO

Keywords:
Silk fiber
Elastin-like polypeptide
Bone repair
Cartilage repair

ABSTRACT

Silk fibroin (SF) is considered biocompatible and biodegradable for osteochondral repair. However, it lacks a bioactive domain for cell adhesion, proliferation and differentiation, limiting its therapeutic efficacy. To revamp SF as a biomimicking and bioactive microenvironment to regulate cell behaviours, we engineered an elastin-like polypeptide (ELP, Val-Pro-Gly-Xaa-Gly) to modify SF fibers via simple and green dehydrothermal (DHT) treatment. Our results demonstrated that the ELP successfully bound to SF, and the scaffold was reinforced by the fusion of the silk fiber intersections with ELP (S-ELP-DHT) via the DHT treatment. Both bone mesenchymal stem cells (BMSCs) and chondrocytes exhibited improved spreading and proliferation on the S-ELP-DHT scaffolds. The *ex vivo* and *in vivo* experiments further demonstrated enhanced mature bone and cartilage tissue formation using the S-ELP-DHT scaffolds compared to the naked SF scaffolds. These results indicated that a recombinant ELP-modified silk scaffold can mimic three-dimensional (3D) cell microenvironment, and improve bone and cartilage regeneration. We envision that our scaffolds have huge clinical potential for osteochondral repair.

1. Introduction

Osteochondral defects involve damage to the articular cartilage and the underlying subchondral bone [1]. They severely affect the daily activities of patients because of significant joint pain and limited joint mobility. Due to the complicated structure and components of cartilage tissues, as well as its avascular nature, low cell density and metabolic activity, osteochondral regeneration are still problematic within the clinical setting [2]. Currently, several treatment options including autograft transplantation and autologous chondrocyte implantation are available to orthopaedic surgeons. These options, however, are limited by donor site morbidity, insufficient donor supply and incomplete integration. As an alternative strategy, tissue engineering has emerged for osteochondral regeneration via promotion of tissue growth by integrating cells, signalling molecules and an artificial environment based on biomaterial scaffolds [3–5].

Synthetic polymers like polyglycolic acid (PGA), polylactide acid (PLA) and polycaprolactone (PCL) are frequently used for cartilage and osteochondral repair owing to their mechanical strength and controllability [6]. However, direct usage of these materials for cartilage repair remains challenging due to high infection rates, foreign body reaction and side effects of acidic degradation byproducts (e.g., inhibition of cartilage regeneration) [7]. Naturally occurring materials like collagen, fibrin, hyaluronic acid, chitosan and silk fibroin (SF), do not possess the-above-mentioned weaknesses and can better match cartilage biological properties [8]. Among these natural polymers, SF, derived from *Bombyx mori* cocoons, is an attractive scaffold material thanks to its versatile processability, slow degradation, strong mechanical properties and favourable biocompatibility [9–11]. It can be readily fabricated into different material formats including hydrogels, tubes, sponges, fibers, microspheres and thin films for various tissue engineering applications [12–15]. However, compared to collagen, an extracellular matrix (ECM) component, SF lacks cell binding domains, making it less ideal as a scaffold to recruit and retain an adequate quantity of bone marrow stem cells (BMSCs) or chondrocytes from subchondral bone to fill the defect area and facilitate the osteochondral regeneration [13,16].

To facilitate SF with improved cell adhesion properties, ECM components like collagen, chondroitin sulfate and Arg-Gly-Asp (RGD) have been employed, but the modified scaffolds only support chondrogenesis after adding signaling molecules like transforming growth factor-β

Peer review under responsibility of KeAi Communications Co., Ltd.
* Corresponding author.
** Corresponding author.
E-mail addresses: xin.zhao@polyu.edu.hk (X. Zhao), chenfl@nwu.edu.cn (F. Chen).

https://doi.org/10.1016/j.bioactmat.2020.09.003
Received 21 July 2020; Received in revised form 3 September 2020; Accepted 4 September 2020

(TGFβ) [17–21]. This is disadvantageous as the molecule release from natural materials is usually quick (within a few days), limiting their long-term therapeutic efficacy. Here, we propose to modify the SF scaffolds using elastin-like polypeptides (ELPs). This is because (1) ELP contains repeated blocks of $(Val\text{-}Pro\text{-}Gly\text{-}Xaa\text{-}Gly)_n$ based on elastin (an essential component of ECM), where Xaa can be any amino acid except proline to create a cell-friendly environment) [22–26]. (2) ELP is beneficial for the maintenance of the chondrocyte phenotype, as demonstrated by the accumulation of collagen type II and sulfated-glycosaminoglycans (sGAG); and (3) it can improve the differentiation of BMSCs or adipose tissue derived stem cells (ADSCs) towards a chondrogenic lineage without the addition of chondrocyte-specific growth factors [23,27,28]. We believe this is an intriguing direction as it avoids incorporation of growth factors and various potential side effects caused by the local release. We hypothesize that the ELP modified SF scaffolds will have enhanced cell adhesion and osteochondrogenesis *in vitro* and *in vivo*.

In the present study, we modified SF fibers with an ELP ($(VPGVG)_{50}$) using dehydrothermal (DHT) treatment. DHT treatment was the most widely adopted physical crosslinking method due to its low cost, low-cytotoxicity and negligible influence on the resulting scaffold structure [29]. The DHT could not only crosslink ELP onto the surface of SF fibers, but crosslink the intersections of each SF fiber, increasing the scaffold's bioactivity and mechanical properties (Fig. 1). Such facile design combining the advantages of silk and ELP together by simple DHT treatment, represents an environment-friendly strategy and possesses high reproducibility. The obtained scaffolds demonstrated the porous and robust structure of SF fibers, and enhanced adhesion and differentiation of BMSCs and chondrocytes due to the presence of ELP. Furthermore, the *in vivo* experiments validated that our ELP modified SF scaffolds bolstered osteochondral regeneration. Thanks to its simple and streamlined design as well as its robust cartilage and bone regeneration capability, we envision that our ELP modified SF scaffolds will help translate the basic research findings into clinical therapy and benefit patients who suffer from osteochondral defects, reducing the burden from families and society.

2. Materials and methods

2.1. Materials and reagents

All chemicals and solvents used for material preparation were of analytical grade and purchased from Sigma-Aldrich (UK), unless otherwise stated. In addition, all reagents used for cell culture, including Dulbecco's Modified Eagle's Media (DMEM), fetal bovine serum (FBS), antibiotics, trypsin and collagenase type II were purchased from Gibco (USA). All primary and secondary antibodies used for immunohistochemistry were from Abcam (UK) and Invitrogen (USA).

2.2. Preparation and characterization of ELP modified SF scaffolds

2.2.1. Preparation of ELP

The ELP ($(VPGVG)_{50}$) was expressed and purified using standard recombinant protein technology as previously reported with some modifications [3]. Briefly, the protein sequences were cloned into pET 28a plasmids, expressed in *Escherichia coli* strain BL21 (DE3), and induced with 1 mM isopropyl β-D-1-thiogalactopyranoside (IPTG) at an OD_{600} of 0.8 for 4 h. The harvested cell pellets were suspended, lysed by sonication, and purified by ion exchange chromatography (IEC). The protein molecular weight and purity were confirmed by using sodium dodecyl sulfate-polyacrylamide gel electrophoresis (SDS-PAGE). The purified ELP was dialyzed three times (10,000 molecular weight cut-off, 36 h, 4 °C, deionized water) to desalt. The ELP was then lyophilized and stored in sealed centrifuge tubes at 4 °C until use.

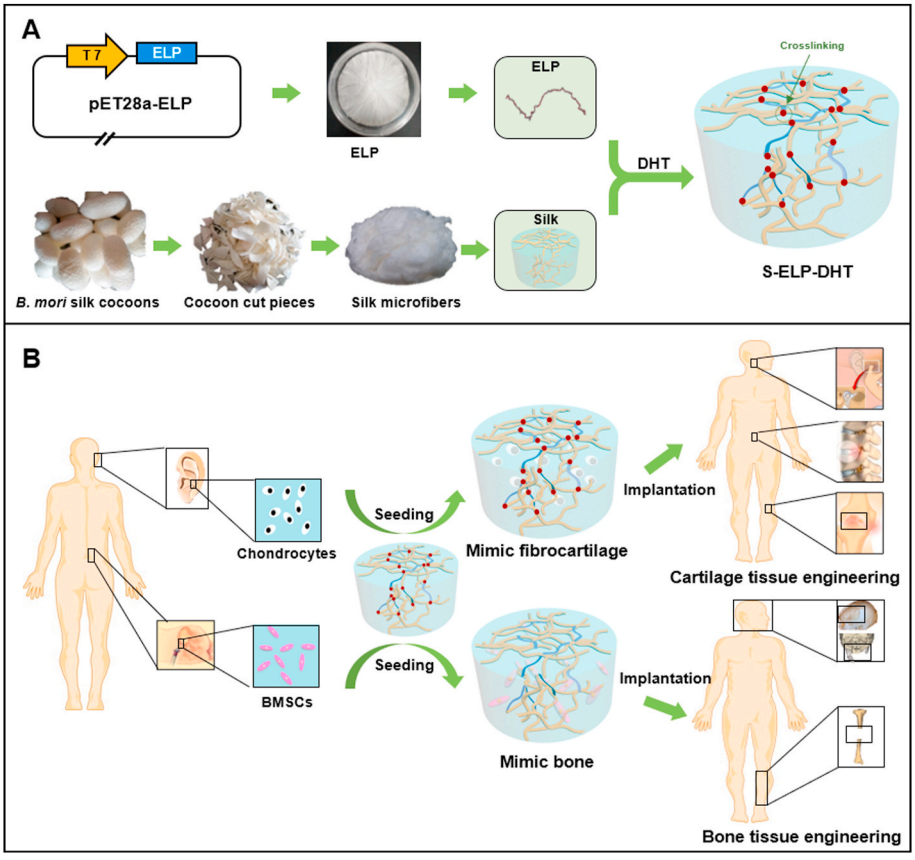

Fig. 1. Schematic representation of (A) S-ELP-DHT scaffold preparation and (B) its potential application in cartilage or bone tissue engineering. S-ELP-DHT scaffold was fabricated with silk, ELP and crosslinked by DHT treatment. By seeding chondrocytes or BMSCs from patients onto the S-ELP-DHT scaffold, a mimetic fibrocartilage or bone can be obtained for *in vivo* implantation to promote cartilage or bone regeneration.

2.2.2. Preparation of SF fibers

Firstly, *B. mori* cocoons were boiled in aqueous sodium carbonate solution (0.5%, w/v) for 2 h, and washed with distilled water to remove sericin. Then, micron-sized, non-immunogenic silk fibers were fabricated according to the published methods [30]. Briefly, 0.35 g of dried, degummed silk fibers were incubated in a 17.5 mol/L NaOH solution for 180 s. The reaction was quenched with deionized water and the SF fibers were washed repeatedly. Fibers were subsequently obtained by lyophilization, and the dried fibers were stored under ambient conditions until use.

2.2.3. Fabrication of ELP modified SF scaffolds

To fabricate the ELP modified SF scaffold, we firstly prepared the SF and ELP complex. Briefly, 10 mg SF fibers were soaked in 75% ethanol, air-dried overnight, and then immersed into sterilized 1 mL ELP solution (1% w/v). After lyophilization, The SF-ELP (S-ELP) complex was obtained and stored at 4 °C for further use. Next, according to previously reported protocol [31], we performed DHT treatment of the S-ELP complexes. When the S-ELP complexes are heated up to a critical temperature, crosslinked bonds between the chains of amino acids present in the SF and ELP molecules would form by esterification of carboxyl and hydroxyl groups and amidation between carboxyl and amino groups. Briefly, S-ELP complexes were placed onto an open polytetrafluoroethylene plate in a vacuum oven (VacuCell 22, MMM, Germany) under a vacuum of 0.05 bar. The exposure period and crosslinking temperature were varied to determine the effects of DHT crosslinking on the S-ELP scaffolds. We found that a crosslinking temperature of 60 °C and an exposure period of 48 h could significantly increase the compressive modulus of the S-ELP scaffold without changing the structure of the ELP (the ELP structure would significantly change over 64–66 °C due to the degradation of β-sheet in the ELP). Therefore, we chose a crosslinking temperature of 60 °C and an exposure period of 48 h in the following study. The treated samples (S-ELP-DHT) were then freeze-dried at −80 °C.

2.2.4. Characterizations of scaffolds

In this study, we prepared four types of scaffolds, namely ELP, SF, S-ELP and S-ELP-DHT. ELP and SF represent the pure elastin-like polypeptide and silk scaffold, respectively. S-ELP represents silk-ELP composite scaffold without DHT treatment, while S-ELP-DHT stands for composite scaffold with DHT treatment. To confirm the successful preparation of these scaffolds, Fourier transform infrared (FTIR) spectra were obtained using a Nicolet 5700 spectrometer (Thermo, USA) with 4 cm^{-1} resolution in the range from 4000 to 4000 cm^{-1}. Then, the surface morphology of these scaffolds was observed using scanning electron microscope (SEM, S–3400 N, Hitachi, Tokyo, Japan) at an accelerating voltage of 10 kV. To examine the effects of the DHT on the hydrophilicity of the S-ELP scaffolds, surface wettability was characterized via static water contact angle measurements using the sessile drop method. The contact angles of the water droplets on the samples were detected at room temperature using an optical goniometer (OCA15EC, Data Physics Company Ltd., Germany).

The *in vitro* degradation rate of the scaffolds was tested according to a previously described method [32]. Briefly, the scaffolds were placed in one well of the six-well plate containing 5 mL of pseudo-physiological solution (DMEM with 1% penicillin-streptomycin) and then incubated at 37 °C, 5% CO_2 and 95% relative humidity for 60 days. The weight of initial dry scaffolds before immersion was recorded as W_0. At different predetermined time points, the scaffolds were removed from the solution and washed three times with double-distilled water to remove inorganic salts. After air-dry in a 37 °C incubator for 24 h, the samples were weighted and recorded as W_t. The remaining weight was evaluated according to the equation: remaining weight (%) = $W_t/W_0 \times 100\%$. Four independent samples of each scaffold were used for degradation test at each time point.

The ELP release profile of each scaffold (S-ELP and S-ELP-DHT) were measured by immersing the samples into 1 mL phosphate-buffered saline (PBS) and incubated at 37 °C for 7 days. At the pre-set time point, 20 μL supernatant was collected and analyzed using the BCA Protein Assay Kit (Thermo Pierce, USA), while same volume of fresh PBS was supplemented to continue the test. Four independent samples of each scaffold were used at each time point.

The mechanical properties of the scaffolds were investigated using a biomechanical analyzer (Instron-5542, Canton, MA, USA). All samples (ELP, S, S-ELP and S-ELP-DHT) with dimension of 10 mm (diameter) x 5 mm (height) were compressed at a constant compressive strain rate of 0.5 mm/min at room temperature until failure (n = 4). The compressive modulus of each sample was calculated from its compressive stress (σ)-strain (ε) curve.

2.3. Cell isolation and cell culture

2.3.1. MSC isolation and culture

BMSCs (rabbit source) were isolated and cultured according to our previously reported method [33]. One-month-old New Zealand white rabbits were obtained from the animal holding unit of Four Military Medical University (FMMU). The procedure of harvesting bone marrow samples was in agreement with Institutional Animal Care and Use Committee (IACUC), and approved by the Animal Ethics Committee of Northwest University of China (ACUC2013015). Briefly, the obtained bone marrow was suspended and cultured in DMEM containing 10% FBS, 272 μg/mL L-glutamine and 100 U/mL penicillin and 100 U/mL streptomycin. The culture media were changed every 3 days. The BMSCs were digested using 0.25% trypsin before forming a confluent monolayer, and harvested by centrifugation. In this study, the second passage of BMSCs were used.

2.3.2. Chondrocyte isolation and culture

Rabbit chondrocytes were isolated and cultured according to our previously described method [34]. All rabbits were anesthetized with ketamine (40 mg/kg) and xylazine (5 mg/kg) via intramuscular injection. The auricle cartilage was obtained from ear roots, minced into small fragments (about 2 mm^3), rinsed three times with PBS supplemented with 100 U/mL penicillin and 100 U/mL streptomycin. Then, samples were digested in DMEM containing 0.2 wt/v% collagenase type II at 37 °C for 12 h. The digested cell suspension was subsequently filtered through a 250 mm nylon mesh filter to remove matrix debris before centrifugation at 1000 rpm for 5 min. The isolated cell pellet was washed two times with PBS and resuspended in DMEM containing 10% FBS, L-glutamine (272 μg/mL), and ascorbic acid (5 μg/mL). Chondrocytes at passage 2–3 were used for this study.

2.4. In vitro biocompatibility of ELP modified SF scaffolds

2.4.1. Cell adhesion

Different cylindrical scaffolds (SF, S-ELP and S-ELP-DHT) with a diameter of 5 mm and a height of 3 mm were first prepared and placed in a 24-well plate. BMSCs or chondrocytes were seeded onto the top surface of each scaffold at a density of 2×10^7 cells/mL (200 μL suspension, a total of 4×10^6 cells), and then cultured in an incubator to ensure adequate cell adhesion to scaffolds. After culture for 6, 12 and 24 h, the samples were removed from culture medium, rinsed twice with PBS, fixed with 2.5% glutaraldehyde at 4 °C for 30 min and finally dehydrated with increasing concentrations of ethanol solutions (30–100%). Scaffolds were then air-dried, sputtered with gold-palladium, and analyzed with SEM. Next, the number of cells adhered onto the scaffolds was evaluated using PicoGreen® DNA quantification assay (Thermo Fisher Scientific) after removal of loosely adherent or unbound cells by washing with PBS. Cell seeding efficiency was calculated using the following equation: Cell seeding efficiency (%) = (Total DNA content of cells in each scaffold)/Total DNA content of initially seeded cells × 100% [35].

2.4.2. Cell proliferation

BMSC or chondrocyte proliferation on the scaffolds was investigated using Cell Counting Kit-8 (CCK-8) assay kit after 1, 3, 5 and 7 days of

incubation. Briefly, the samples were washed twice with PBS after removing from the culture medium. Subsequently, 400 μL of fresh phenol red-free medium with a 40 μL CCK-8 reagent was added to each sample, and then incubated for 3 h in an incubator at 37 °C with 5% CO_2. 100 μL of incubated medium from each sample was transferred to a 96-well culture plate, and shaken for 2 min. The absorbance was measured at 450 nm using a microplate reader (Bio-Rad, USA). All experiments were performed in quadruplicate. To observe the cells adhering to the scaffolds after culture for 3, 5 and 7 days, the samples were first fixed with 4% (v/v) paraformaldehyde. Then, the cytoskeleton of BMSCs and chondrocytes was stained with phalloidin-Cy3 (actin, red) and phalloidin-FITC (actin, green), respectively, while their nuclei were stained with 4,6-diamidino-2-phenylindle (DAPI). Fluorescent images of samples were viewed by a confocal laser scanning microscope (FV1000, Olympus Corporation, Tokyo).

2.4.3. Osteogenesis- and chondrocyte phenotype-related gene expression

The gene expression of osteoblast differentiation markers (runt-related transcription factor 2 gene (*Runx2*), alkaline phosphatase gene (*ALP*) and osteopontin gene (*OPN*)) in BMSCs, and chondrocyte phenotype-related markers (collagen type I gene (*Col I*), collagen type II gene (*Col II*), and the aggrecan gene (*AGG*)) in chondrocytes were measured using reverse transcription-polymerase chain reaction (RT-PCR). Briefly, BMSCs or chondrocytes were seeded onto the surface of different scaffolds (SF, S-ELP and S-ELP-DHT) and cultured for 3, 7 and 14 days. Then, cells were collected from each sample, and the total RNA was isolated from chondrocytes or BMSCs using TRIzol Reagent (Invitrogen, Carlsbad, CA, USA). Complementary DNA (cDNA) was synthesized from 1 μg of RNA using the TaKaRa RT-PCR Kit (TaKaRa Bio Inc., Japan). The thermal cycling parameters for RT-PCR conditions were showed as follow: initial denaturation at 94 °C for 3 min; 30 cycles of 94 °C for 40 s, 60 °C for 40 s and 72 °C for 80 s; and a final extension at 72 °C for 5 min. The glyceraldehyde 3-phosphate dehydrogenase gene (*GAPDH*) was used as the internal control. The primer sequences used for this study were listed in Table S1. The PCR products were visualized using 1.5% agarose gels. Band intensity was quantified using Bandscan software. The grey values of bands were normalized relative to those of *GAPDH*.

2.5. Animal models

All animal experiments were performed in accordance with Guiding Principles of the Care and Use of Animals and approved by the IACUC of Northwest University of China.

2.5.1. Subcutaneous implantation

Healthy BALB/c nude mice (6–8 weeks old and weighing approximately 18–22 g) were anesthetized with intraperitoneal injection of 10% chloral hydrate (300 mg/kg). After aseptic preparation, the skin on the back of each mouse was incised and a subcutaneous pocket was made. Four different groups of BMSCs- or chondrocytes-loaded SF and S-ELP-DHT scaffolds (i.e., SF/BMSCs, SF/chondrocytes, S-ELP-DHT/BMSCs and S-ELP-DHT/chondrocytes) were prepared as described in section 2.4.1, and then implanted into the subcutaneous pockets. After 1 and 2 months of implantation, all nude mice were sacrificed by neck dislocation, and the samples were harvested. After macroscopic observation, the samples were fixed by 4% (v/v) paraformaldehyde for subsequent analysis.

2.5.2. Articular joint drilling surgery

Articular surgery was performed as previously described [32]. 16 rabbits were randomly divided into four groups: negative control (untreated defect), positive control (normal knee joint), SF and S-ELP-DHT. Briefly, the rabbits were anesthetized with intraperitoneal injection of pentobarbital sodium (30 mg/kg) and maintained with 3% isoflurane. A parapatellar incision was made to expose the knee joint of the rabbits, and then the patella was dislocated laterally to expose the anterior articular surface of the distal femur. A full-thickness osteochondral defect with diameter of 4 mm and depth of 4 mm was created in the trochlear groove of the femur using an electrical trephine. After irrigating with sterile saline solution, SF or S-ELP-DHT scaffold was carefully implanted into the osteochondral defects. Finally, the wound was closed by suturing the knee joint capsule and the skin, and the penicillin was given intramuscularly for prophylactic infection. After 2 months post-implantation, the rabbits were sacrificed and the regenerated tissue scaffolds were retrieved.

2.5.3. Micro-computed tomography (micro-CT)

The samples were subjected to morphological and quantitative examination using a micro-CT system (Y.Cheetah, YXLON, Germany) with the following settings: 80 kV voltage, 50 μA electric current and 10 μm resolution. Based on the serial-scanned images, the 3D isosurface images were reconstructed using VG Studio software (version 2.2). The threshold used in this study was 0–4000 Hounsfield units (Hu) for bone tissue according to the threshold calculations for the samples. The bone volume fraction (BVF, the ratio between the bone volume and the total tissue volume) and the bone mineral density (BMD, the mass of bone per unit volume) of the samples were calculated.

2.5.4. Histological and immunohistochemical analysis

The samples were fixed in 4% paraformaldehyde for 24 h and decalcified in 5% formic acid for 5 days. Then, these samples were dehydrated in a graded series of alcohol solutions, embedded in paraffin, and cut into 7-μm-thick sections. The sections were stained with haematoxylin and eosin (H&E), toluidine blue (TB), safranin O (S–O), and Masson's trichrome staining (MTS) to evaluate new cartilage and bone formation [36].

For the immunohistochemical analysis, the sectioned slides were incubated overnight in a humidified chamber with primary antibodies of anti-Col I antibody, anti-Col III antibody, anti-CD 31 antibody, and anti-Col X antibody according to the manufacturer's instruction. Then, the sections were rinsed with PBS and incubated with Alexa Fluor® 594 anti-mouse secondary antibody or Alexa Fluor® 488 anti-mouse secondary antibody before being stained with DAPI. The fluorescence images of the stained sections were obtained using a confocal laser scanning microscope (FV1000, Olympus Corporation, Tokyo).

2.5.5. Biomechanical and biochemical evaluations

After implantation for 1 and 2 months, the regenerated tissues were harvested from the chondrocytes-loaded samples of subcutaneous implantation using a trephine (5 mm in inner diameter). The elastic cartilage and the fibrocartilage of rabbits were used as positive controls. Biomechanical evaluation was carried out by static compression using a biomechanical analyzer (Instron-5542, Canton, MA, USA) according to the method described previously [37]. Briefly, a constant compressive strain rate of 0.5 mm/min was applied on the samples (5 mm in diameter and 3 mm in height) until 80% maximal deformation was achieved. The compressive modulus of the tested tissue was calculated based on the slope of the stress-strain curve. Four independent samples were tested for each group. After the mechanical testing, the tissue samples were collected, rinsed in PBS, minced and homogenized using a glass grinder. The glycosaminoglycan (GAG, a cartilage-specific matrix component) content in the regenerated tissues was measured using a Rabbit GAG enzyme-linked immunosorbent assay (ELISA) Kit (TaKaRa Bio Inc., Japan) according to protocol provided by the manufacturer.

2.6. Data analysis

All experiments were carried out at least in quadruplicate if not specified. All data were presented as mean ± standard deviation (SD). Statistical analysis was performed using SPSS version 15.0 software (SPSS Inc., Chicago, USA). The statistical differences were analyzed by

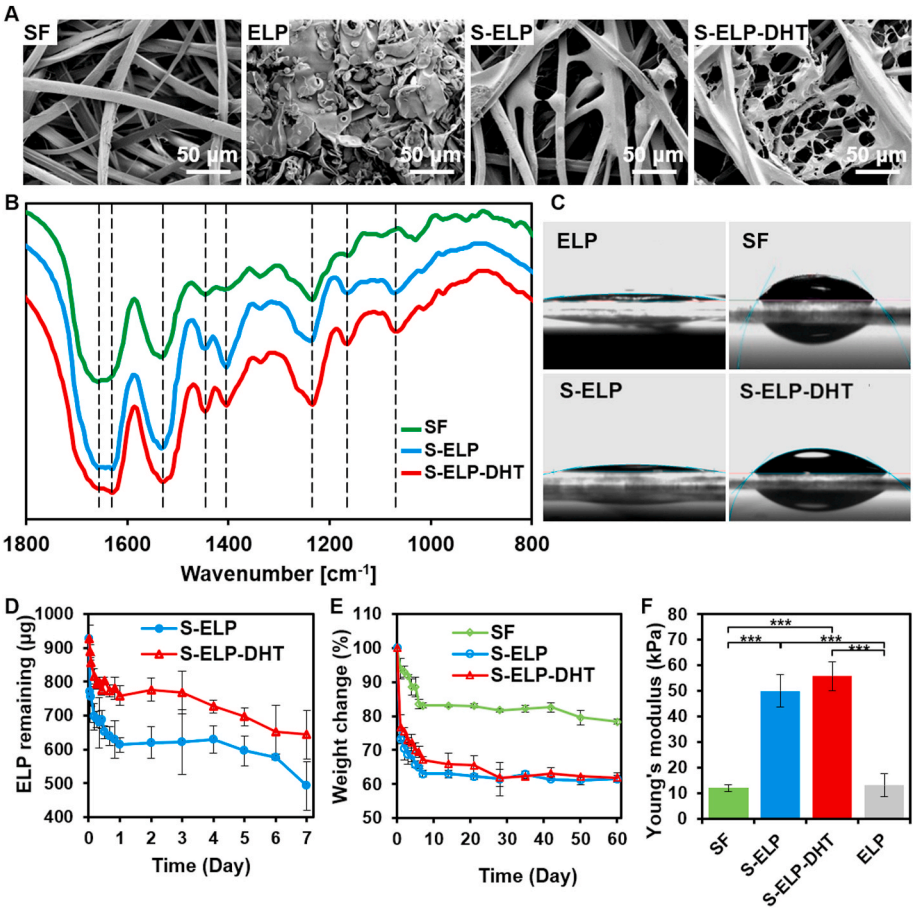

Fig. 2. Characterization of the scaffolds. (A) SEM micrographs of pure silk fibroin (SF), ELP, S-ELP and S-ELP-DHT scaffolds. (B) FTIR spectra of SF, S-ELP and S-ELP-DHT scaffolds. (C) Water contact angle assessments of ELP, SF, S-ELP and S-ELP-DHT scaffolds. (D) The ELP release rate from S-ELP and S-ELP-DHT was monitored using a BCA Protein Assay Kit. (E) Mass loss profile of SF, S-ELP and S-ELP-DHT scaffolds characterized as remaining weight with time. (F) Compressive modulus of pure ELP, SF, S-ELP and S-ELP-DHT scaffolds. Data were represented as mean ± SD, and analyzed by one-way ANOVA (n = 4 for each group, ***$p < 0.001$).

one-way analysis of variance (ANOVA) with post hoc tests. A p value of < 0.05 was considered statistically significant.

3. Results and discussion

3.1. Preparation and characterization of ELP-silk microfiber complexes

In present study, ELP was designed and produced to modify the SF scaffolds (Figs. S1A–C). The microarchitecture of the silk and ELP complexes were examined using SEM. Silk, S-ELP, and S-ELP-DHT scaffolds exhibited loose and porous fibrous structure (Fig. 2A). In addition, we observed that ELP physically adhered to the silk in the S-ELP complex with noticeable fusion of ELP with the surrounding silk microfibers. In contrast, the ELP formed a thin film with internal porosity between SF fibers in the S-ELP-DHT complex, which could supply more space for cells attachment. The above results have indicated that the ELP was able to bind with SF fibers by DHT treatment, resulting in a smooth appearance along the surface of the SF fibers. FTIR was further used to investigate the chemical structure change of the scaffolds after the physical adherence of ELP and DHT treatment (Fig. 2B). We found that the SF surface produced a peak at 1655 cm^{-1} corresponding to the stretching vibration (ν) of C═O (amide I), and a peak at 1530 cm^{-1} corresponding to the in-plane bending vibration (δ) of N–H (amide II); adherence of the ELP to the silk resulted in a new peak at 1630 cm^{-1} corresponding to δ N–H (amide II), and new peaks at 1166 cm^{-1} and 1069 cm^{-1} corresponding to ν C–N; the FTIR spectra of S-ELP and S-ELP-DHT were comparable. These results have suggested the successful adherence of ELP to silk scaffolds and an absence of chemical structural changes during the DHT treatment.

Subsequently, SDS-PAGE analysis was performed to evaluate the protein composition of ELP and SF, with unified molecular weight of approximately 25 and 40 kDa, respectively (Fig. S1D). The hydrophilicity alteration of the sample surface after ELP incorporation and DHT treatment was examined by measuring water contact angles at room temperature (Fig. 2C). We found that the materials surfaces (SF: 55.2 ± 5.2°; S-ELP: 10.7 ± 1.4°; S-ELP-DHT: 39.0 ± 5.5°) were all hydrophilic, which are conducive for cell adhesion. In detail, the water contact angle of SF decreased from 55.2 ± 5.2° to 10.7 ± 1.4° (S-ELP) after adherence of ELP, which may be due to the super-hydrophilic nature of ELP (water contact angle: 9.1 ± 0.2°). However, after DHT treatment, the S-ELP-DHT samples became more hydrophobic, with water contact angle dramatically increasing to 39.0 ± 5.5°. Such change possibly resulted from the formation of ester and amide bonds during the DHT treatment by either esterification or amide reactions, which decreases the amount of the free amine, carboxyl, and hydroxyl groups [38].

Next, we evaluated the ELP release rates from the S-ELP and S-ELP-DHT scaffolds by immersing the samples into PBS (Fig. 2D). Compared with S-ELP, S-ELP-DHT showed a more stable and sustainable ELP release, demonstrating the successful conjugation of ELP to the SF surface after the DHT treatment. We further analyzed the mass loss profile of silk, S-ELP, and S-ELP-DHT scaffolds. As showed in Fig. 2E, S-ELP and S-ELP-DHT samples degraded faster than the pure silk during the 60 days of immersion in DMEM. This may be attributed to the disruption of structural integrity of fibroin protein after introduction of ELP, which exposed fibroin molecules onto the composite surface and facilitates the invasion of water molecules.

Mechanical properties of materials like matrix stiffness play a crucial role in regulating cell behaviours and promoting osteochondrogenesis. Therefore, we subsequently characterized the mechanical performances of the prepared scaffolds using compression testing. Our results showed that incorporation of ELP into silk fibers significantly improved the mechanical property of the composite scaffolds, with compressive moduli of S-ELP and S-ELP-DHT reaching up to 49.98 ± 6.25 kPa and 55.73 ± 5.76 kPa, respectively (Fig. 2F). The SEM observation

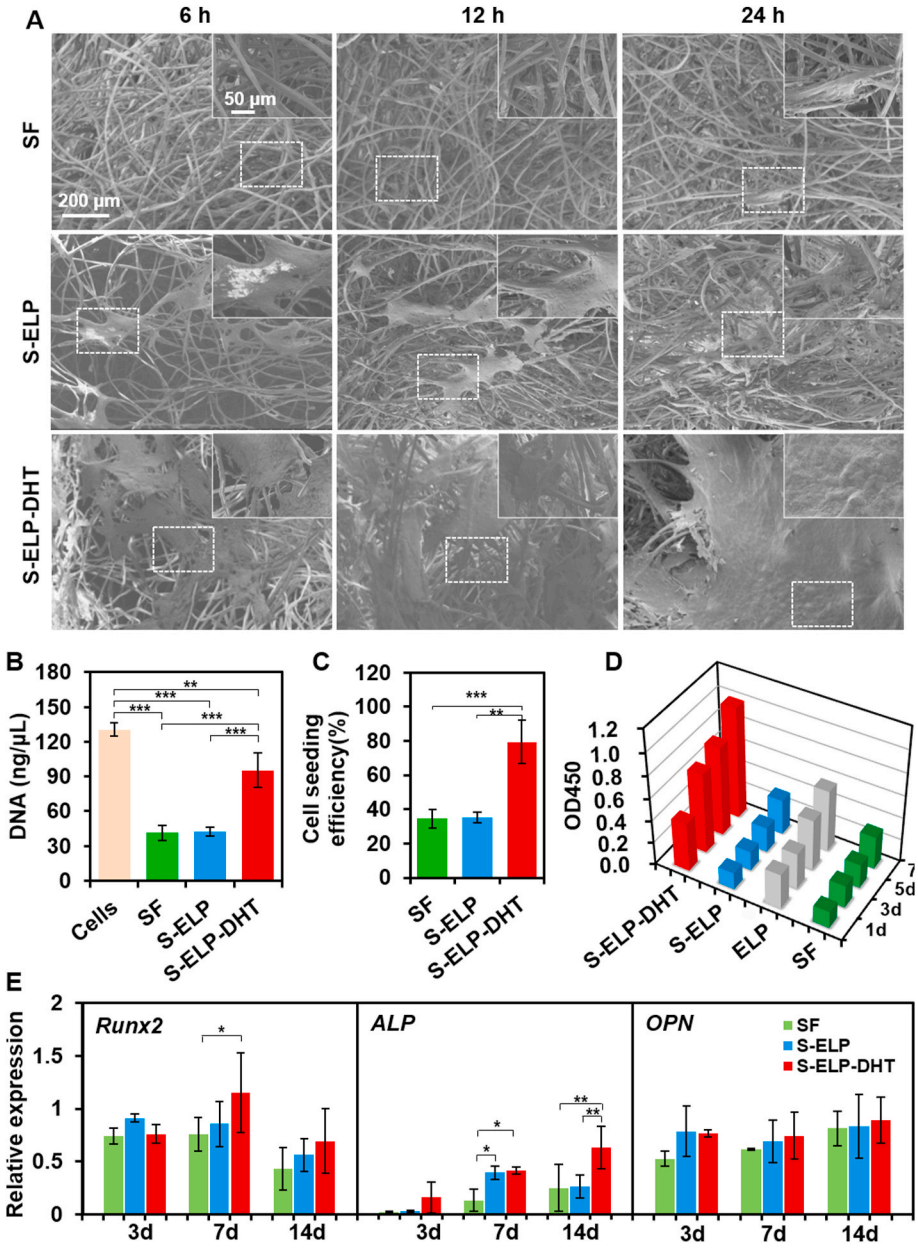

Fig. 3. Adhesion, proliferation and osteoblast differentiation of BMSCs on the SF, S-ELP and S-ELP-DHT scaffolds. (A) SEM images of BMSCs seeded on different scaffolds after 6, 12 and 24 h of culture. (B) The DNA content of BMSCs cultured for 24 h on different scaffolds detected using PicoGreen DNA quantitation assay. (C) The BMSC-seeding efficacy of SF, S-ELP and S-ELP-DHT scaffolds. The initially seeded BMSCs (cell number of 4×10^6) were used as the control group. (D) Proliferation of BMSCs on SF, ELP, S-ELP and S-ELP-DHT scaffolds after 1, 3, 5 and 7 days of culture measured by CCK-8. (E) RT-PCR analysis of osteogenesis-related marker gene expressions including *Runx2*, *ALP* and *OPN* in BMSCs after culture with different scaffolds for 3, 7 and 14 days. *GAPDH* was used as an internal control. Data are presented as mean ± SD and analyzed by one-way ANOVA (n = 4 for each group, $^*p < 0.05$, $^{**}p < 0.01$, $^{***}p < 0.001$).

indicated that ELPs wrapped around the intersections of the silk fibers in the S-ELP and S-ELP-DHT scaffold (Fig. 2A), which may be the main reason for that the compressive moduli of S-ELP scaffold (49.98 ± 6.25 kPa) and the S-ELP-DHT scaffold (55.73 ± 5.76 kPa) were significantly higher than that of the naked silk fibers (11.97 ± 1.25 kPa, n = 4, p < 0.001, Fig. 2F). Also, there was no significant difference found in modulus between the S-ELP scaffold and the S-ELP-DHT scaffold (n = 4, p > 0.05, Fig. 2F). Previous studies have reported that the compressive moduli of the ELP composite materials prepared via photocrosslinking or chemical crosslinking methods were in the range of 3–13 and 4–11 kPa, respectively [39,40]. Recently, Prof Kaplan's lab constructed a recombinant fusion SELP using the silk sequence GAGAGS and elastin sequence GVGVP [41,42]. The authors found that after the recombinant SELP was enzymatically crosslinked by horseradish peroxidase (HRP) and hydrogen peroxide (H_2O_2), the compressive modulus of the cross-linked SELP hydrogel was 2.5 ± 0.9 kPa [42]. The compressive modulus of our S-ELP-DHT scaffold crosslinked via DHT treatment was higher than those in previous studies, which may be due to the formation of an interpenetrating network between the SF and the ELP polymers. Such high compressive modulus was highly beneficial for osteochondrogenesis [43]. Overall, the above results demonstrated that the combination of SF and ELP successfully yielded a composite scaffold with excellent degradation and mechanical property, with great potential for osteochondral defect repair.

3.2. *In vitro* biological evaluations of scaffolds

3.2.1. *Biocompatibility*

A tissue engineering scaffold should possess good cytocompatibility that facilitates cell growth and proliferation without eliciting any immune response. Here, we evaluated the *in vitro* biocompatibility of fabricated scaffolds by observing BMSC and chondrocyte attachment and measuring their proliferation on the scaffolds. The morphology of BMSCs and chondrocytes adhered to scaffolds was examined using SEM (Figs. 3A and 4A). Compared with SF and S-ELP scaffolds, BMSCs or chondrocytes were observed to attach with higher density to the S-ELP-DHT scaffolds. Notably, after 24-h cell seeding, the surface of the S-ELP-DHT scaffolds was completely covered with spreading BMSCs. The chondrocytes on the S-ELP-DHT scaffolds also exhibited more obvious pseudopodia and aggregation than those on SF or S-ELP scaffolds. The

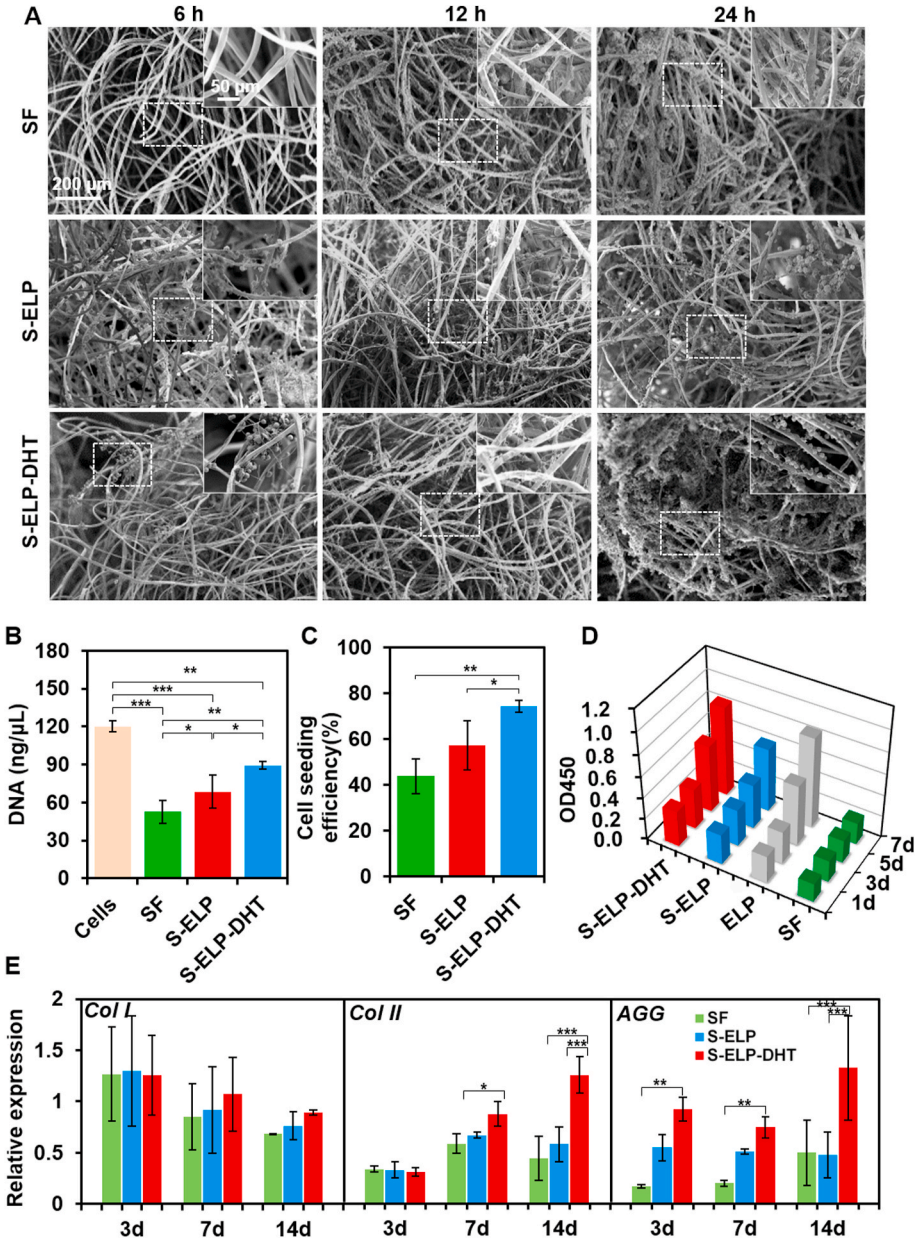

Fig. 4. Adhesion, proliferation and cartilage marker gene expression of chondrocytes on SF, S-ELP and S-ELP-DHT scaffolds. (A) SEM images of chondrocytes seeded on different scaffolds after 6, 12 and 24 h of culture. (B) The DNA content of chondrocytes cultured for 24 h on different scaffolds detected using PicoGreen DNA quantitation assay. (C) The chondrocyte-seeding efficacy of SF, S-ELP and S-ELP-DHT scaffolds. The initially seeded chondrocytes (cell number of 4×10^6) were used as a control. (D) Proliferation of chondrocytes on SF, ELP, S-ELP and S-ELP-DHT scaffolds after 1, 3, 5 and 7 days of culture measured by CCK-8. (E) RT-PCR analysis of chondrocyte phenotype-related marker gene expressions including *Col I*, *Col II* and *AGG* in chondrocytes after culture with different scaffolds for 3, 7 and 14 days. *GAPDH* was used as an internal control. Data are presented as mean ± SD and analyzed by one-way ANOVA (n = 4 for each group, $^*p < 0.05$, $^{**}p < 0.01$, $^{***}p < 0.001$).

number of cells attached to the scaffolds was reflected in its total DNA content (Figs. 3B and 4B). The initially seeded BMSCs or chondrocytes (cell number of 4×10^6) amounted to total DNA content of 130.67 ± 5.77 ng/μL and 120.00 ± 4.36 ng/μL, respectively, which were used as control groups. As showed in Fig. 3B, no significant difference was observed regarding the number of BMSCs attached to the SF (41.33 ± 6.43 ng/μL) and to the S-ELP (42.33 ± 3.79 ng/μL) scaffolds. However, there were significantly more BMSCs adhered to the S-ELP-DHT scaffolds (95.33 ± 15.01 ng/μL, $^{***}p < 0.001$). The BMSC seeding efficiency on the S-ELP-DHT scaffolds (79.44 ± 12.51%) was much higher than on that on the SF (34.44 ± 5.36%, $^{***}p < 0.001$) or on the S-ELP (35.28 ± 3.15%, $^{**}p < 0.01$) scaffolds (Fig. 3C). Similarly, the S-ELP-DHT scaffolds showed obviously more adhered chondrocytes (89.33 ± 3.06 ng/μL) and greater chondrocyte-seeding efficiency (74.44 ± 2.55%) (Fig. 4B and C).

Subsequently, cell proliferation was quantified using CCK-8 assay after incubation for 1, 3, 5 and 7 days on the scaffolds (Figs. 3D and 4D). At each time point, the number of BMSCs on the S-ELP-DHT scaffolds (OD450: 0.43 ± 0.01 at day 1; 0.71 ± 0.03 at day 3; 0.79 ± 0.02 at day 5; 0.99 ± 0.11 at day 7; n = 4) was significantly higher than that on the SF (OD450: 0.15 ± 0.01 at day 1; 0.20 ± 0.02 at day 3; 0.21 ± 0.03 at day 5; 0.29 ± 0.03 at day 7), ELP (OD450: 0.31 ± 0.13 at day 1; 0.32 ± 0.19 at day 3; 0.45 ± 0.14 at day 5; 0.55 ± 0.14 at day 7) and S-ELP scaffolds (OD450: 0.15 ± 0.03 at day 1; 0.17 ± 0.09 at day 3; 0.22 ± 0.11 at day 5; 0.31 ± 0.13 at day 7). At day 1, 5 and 7, the number of chondrocytes on the S-ELP-DHT scaffolds (OD450: 0.33 ± 0.01 at day 1; 0.62 ± 0.01 at day 5; 0.83 ± 0.02 at day 7) was significantly higher than that on the SF (OD450: 0.17 ± 0.01 at day 1; 0.21 ± 0.03 at day 5; 0.20 ± 0.02 at day 7), respectively. Either BMSC or chondrocyte proliferation on the S-ELP-DHT scaffold was better than that on the SF, ELP or S-ELP scaffolds, indicating that the S-ELP-DHT provided a more favourable environment for cell proliferation. The fluorescence micrographs further confirmed more BMSCs and chondrocytes distributed along the fibers of S-ELP-DHT as compared to the SF scaffolds (Fig. S2). These results suggested that the S-ELP-DHT scaffo lds exhibited satisfactory biocompatibility and could support cell adhesion and proliferation after implantation.

To sum up, ELP formed a thin film with internal pores between the SF fibers in the S-ELP-DHT complex (Fig. 2A), which could supply more

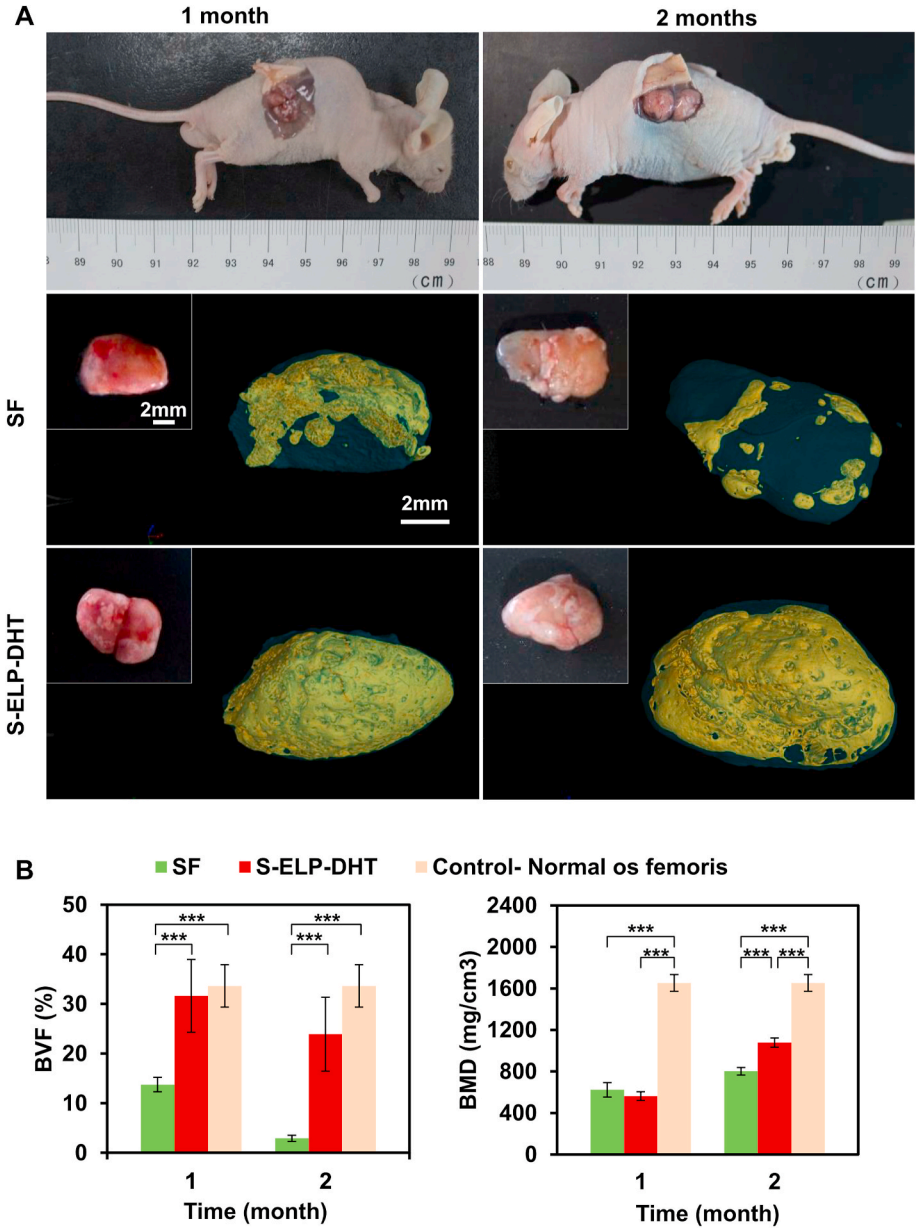

Fig. 5. Ectopic bone regeneration in nude mice. (A) The cell-scaffold constructs (BMSC-seeded SF and BMSC-seeded S-ELP-DHT composite scaffolds) were implanted into subcutaneous tissue of nude mice. After implantation for 1 and 2 months, gross view and micro-CT scanning were performed to analyze the harvested composite scaffolds. Yellow stained area in the 3D reconstructed micro-CT images indicates the new bone tissue. Quantitative analysis of (B) bone volume fraction (BVF) and (C) bone mass density (BMD) of the newly formed bone by micro-CT. Data are presented as mean ± SD and analyzed by one-way ANOVA (n = 4 for each group, $^{***}p < 0.001$).

space for cell attachment. Secondly, ELP as a bioactive protein affecting the behaviours of BMSCs and chondrocytes. Due to the bioactive ELP, the cell adhesion (Figs. 3C and 4C) and proliferation (Figs. 3D and 4D) on the S-ELP-DHT were better than those on the naked silk scaffolds. Because the ELP was lost faster in the S-ELP scaffolds than that in the S-ELP-DHT scaffolds (Fig. 2D), cell adhesion and proliferation on the S-ELP scaffold were less than those on the S-ELP-DHT scaffolds. In a word, both the unique structure of the scaffold and the bioactive ELP are beneficial for adhesion and proliferation of BMSCs and chondrocytes.

3.2.2. *In vitro* osteogenic and chondrogenic capacities

To evaluate the *in vitro* differentiation of BMSCs into osteoblasts on the scaffolds, we measured the expression levels of osteogenesis-related marker genes including *Runx2*, *ALP* and *OPN* (Fig. 3 E and S3). Our results showed that the expression of preosteoblast marker *Runx2* in the S-ELP-DHT was significantly upregulated after 7 days of incubation, although its expression in SF or S-ELP scaffolds was downregulated throughout the experiment. However, *ALP* and *OPN* expressions were continuously upregulated in BMSCs on S-ELP-DHT scaffolds during the whole culture period. Particularly, after 14 days of culture, *ALP* expression was remarkably higher on the S-ELP-DHT scaffolds than that on the SF or S-ELP scaffolds. It has been demonstrated that SF is a favourable scaffold material for bone regeneration due to its tunable degradation rate, good mechanical properties and the ability to induce osteogenic differentiation of BMSCs [44]. In addition, ELP was also found to support attachment, proliferation and osteoblast differentiation of BMSCs because of the exposure of motifs of ELP to the cells. These previous studies correlate well with the findings in our study and support that S-ELP-DHT is a promising candidate material for bone tissue engineering.

Apart from unique osteogenic potential, the scaffolds for osteochondral repair are required to maintain the phenotype of chondrocytes that produce extracellular matrix (ECM) within the scaffolds, contributing to new cartilage tissue formation. It is well-known that *Col I* expression is associated with fibrocartilage or hypertrophic phenotypes, while *AGG* and *Col II*, as the major ECM components of cartilage, are markers of hyaline chondrocyte phenotype [3,45]. Here, we evaluated the expression levels of these cartilage marker genes (*Col I*, *Col II* and *AGG*) of chondrocytes on different scaffolds. As showed in Fig. 4E and Fig. S3, there was no obvious difference in *Col I* expressions among SF, S-ELP and S-ELP-DHT groups, and the *Col I* expression levels in these three groups decreased with culture time. Both *Col II* and *AGG* expression levels were significantly higher in the S-ELP-DHT scaffolds

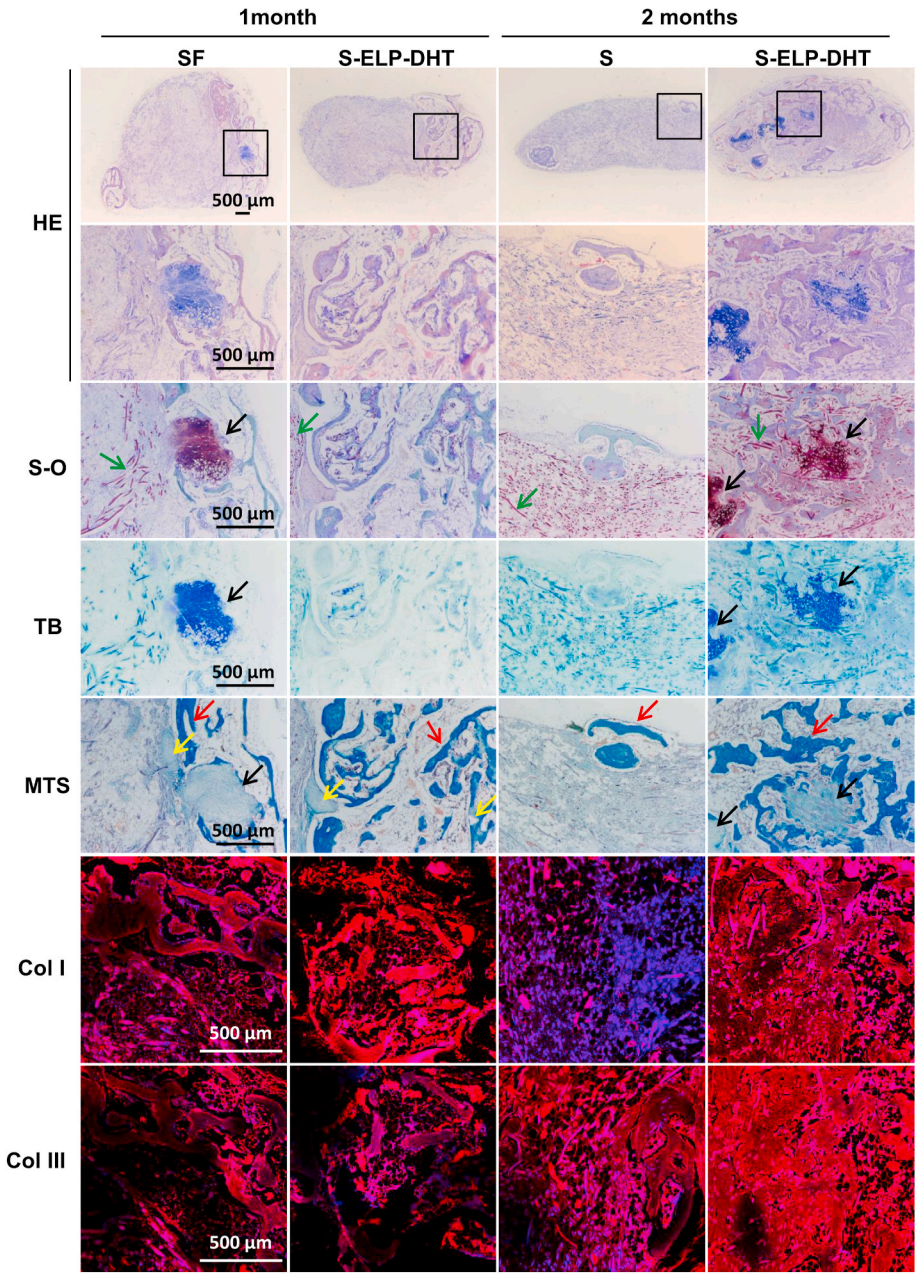

Fig. 6. Histological analysis of BMSC-seeded SF and BMSC-seeded S-ELP-DHT composite scaffolds after implantation into subcutaneous tissue of nude mice for 1 and 2 months. Sections were stained with H&E, Safranin-O (S–O), toluidine blue (TB) and Masson's trichrome staining (MTS), or immunostained for Col I and Col III to evaluate the ECM deposition and the structure of regenerated cartilage and bone tissue. Green arrows indicate SF fibers, black arrows indicate cartilage, yellow arrows indicate calcified cartilage and red arrows indicate bone. The black squares represent the below high magnification images (H&E, S–O, TB and MTS). In the immunostained images, red color represents Col I or Col III while blue color indicates the cell nuclei.

compared with SF and S-ELP groups after 7 or 14 days of culture *in vitro*. To repair articular cartilage injuries, an ideal scaffold should facilitate hyaline cartilage regeneration accompanied with suppression of scar and fibrocartilaginous tissue formation [32]. Our results demonstrated that the S-ELP-DHT scaffolds could improve desirable hyaline cartilage phenotype while reducing the undesirable fibrocartilage phenotype. In addition, these findings are consistent with previous reports that SF can facilitate adhesion and proliferation of chondrocytes and production of cartilaginous matrix *in vitro* [21,46]; ELP can promote the rapid accumulation and retention of a chondrocyte-associated matrix, allowing for the longer-term maintenance of chondrocyte phenotype [47]. Taken all together, our S-ELP-DHT scaffolds have great potential for *in vivo* articular cartilage repair.

3.3. Evaluations of subcutaneous bone and cartilage regeneration

3.3.1. Ectopic bone formation

The feasibility of designed scaffolds to promote *in vivo* bone regeneration was investigated by implanting BMSC-seeded composite scaffolds into the subcutaneous pockets in nude mice for 1 and 2 months. The mice in all groups survived throughout the experiments, and there were no visible inflammatory reactions, infections or extrusions around the implantation sites, indicating the *in vivo* biocompatibility of the scaffolds. After 1 and 2 months of implantation, we found a thin layer of white soft tissue formed on the surfaces of SF and S-ELP-DHT composite scaffolds (Fig. 5A). Notably, the generation of new blood vessels was observed on the S-ELP-DHT at 2 months post-implantation. This is advantageous for steady supply of oxygen and nutrients to the implants and maintenance of the long-term clinical success (Fig. 5A and Fig. S4). Next, micro-CT analysis was performed to assess the new bone formation of the implanted scaffolds (Fig. 5A). From the 3D reconstructed images, it could be clearly found that the S-ELP-DHT scaffolds displayed more significant new bone formation compared to the SF group after 1 or 2 months of implantation. Quantitative micro-CT data analysis further confirmed the markedly higher BVF and BMD values in the S-ELP-DHT scaffolds as compared to SF group (Fig. 5B).

The H&E staining revealed that the new tissues with histologic appearance of osteoid were formed within the scaffolds. With increasing

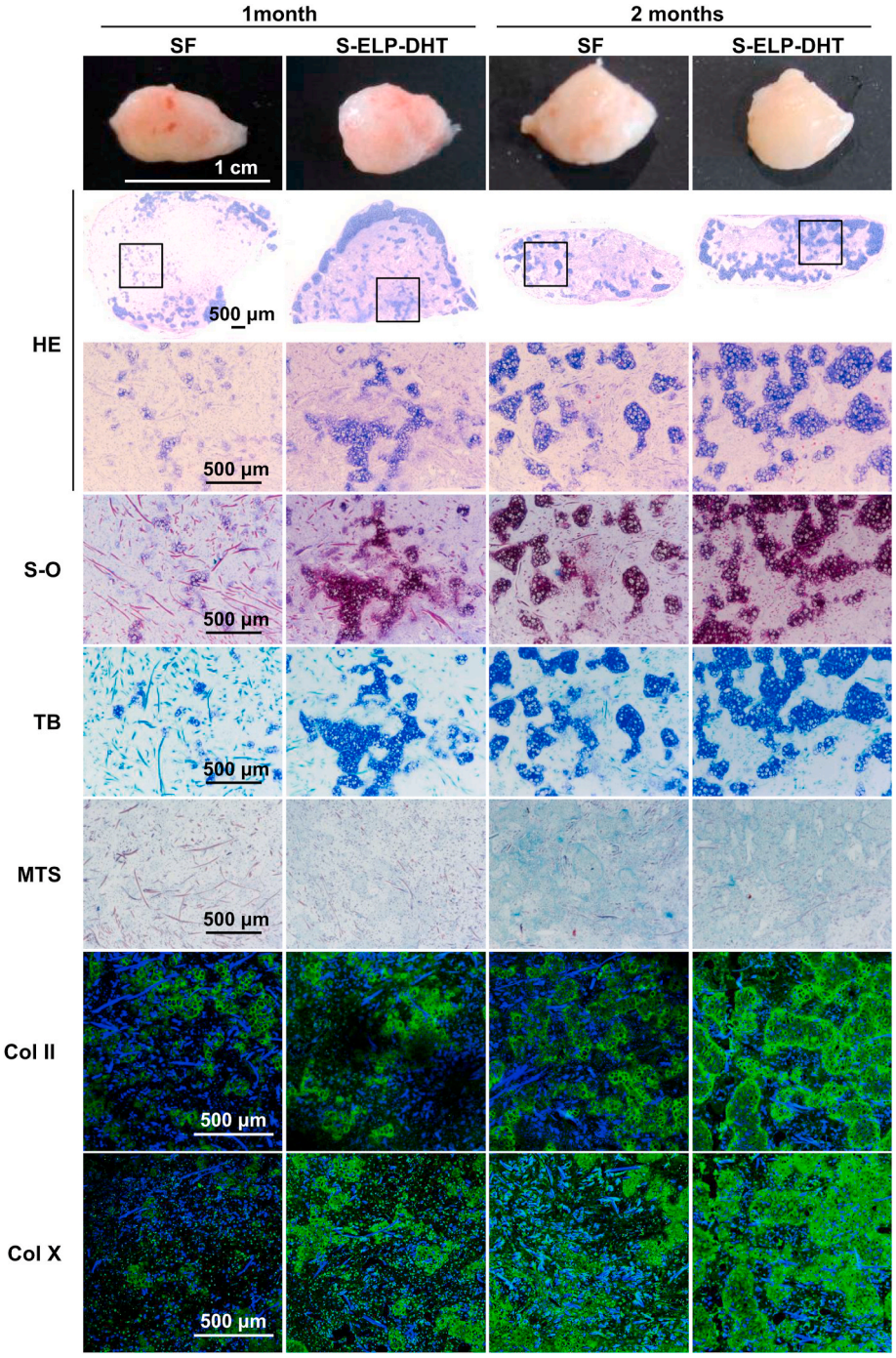

Fig. 7. Ectopic cartilage regeneration in nude mice. Gross view and histological analysis of chondrocyte-seeded SF and S-ELP-DHT composite scaffolds after implantation into subcutaneous tissue of nude mice for 1 and 2 months. Sections were stained with H&E, S–O, TB and MTS, or immunostained for Col II and Col X to assess the ECM deposition and the structure of regenerated cartilage tissue. In the immunostained images, green color represents Col II or Col X while blue color indicates cell nuclei.

in vivo culture time, some parts of the scaffolds were gradually absorbed without eliciting obvious inflammatory cell infiltration (Fig. 6). To gain insight into the effect of BMSC-seeded S-ELP-DHT scaffolds on spatial organization of neo-cartilage formation over time, we performed S–O, TB and MTS staining to estimate the intensity and distribution of newly deposited collagen and polysaccharide by BMSCs (Fig. 6). After 2-month implantation, the S-ELP-DHT scaffolds showed more intense polysaccharide and collagen deposition compared to the SF group. Almost the entire S-ELP-DHT scaffold was remodelled and subsequently filled with polysaccharide at 2 months. These results demonstrated more cartilage ECM formation in the S-ELP-DHT scaffolds than in the SF group (1 or 2 months), suggesting better endochondral ossification. The immunohistochemical staining of osteoblastic-specific markers (Col I and Col III) also showed substantially higher amounts of Col I and Col III deposition in the S-ELP-DHT scaffolds, which further verified that our designed scaffolds could promote endochondral bone formation (Fig. 6 and Fig. S5). Together, these results indicated the S-ELP-DHT scaffolds could effectively promote the osteogenesis of the seeded BMSCs and enhance the new bone tissue regeneration *in vivo*.

3.3.2. Ectopic cartilage formation

Next, we assessed the *in vivo* cartilage regeneration capability of our

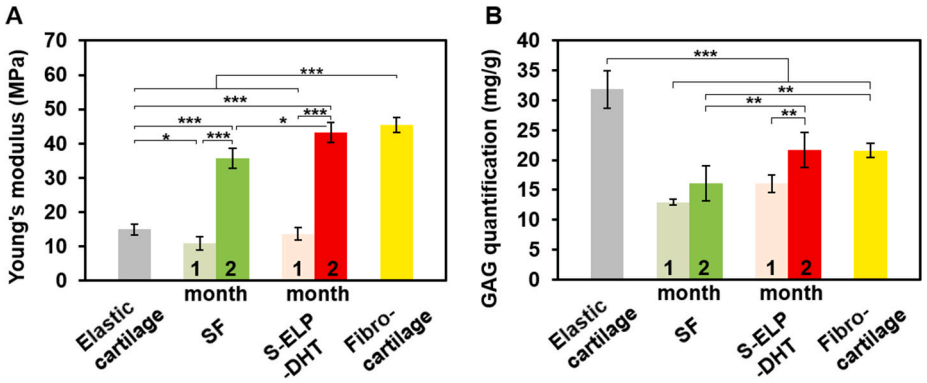

Fig. 8. Biomechanical and biochemical evaluation of chondrocyte-seeded SF and S-ELP-DHT composite scaffolds at 1 and 2 months post-implantation. (A) Dynamic mechanical analysis showing the compressive modulus of chondrocyte-seeded scaffolds. (B) Quantification of GAG content of chondrocyte-seeded scaffolds. Data are presented as mean ± SD and analyzed by one-way ANOVA (n = 4 for each group, $*p < 0.05$, $**p < 0.01$, $***p < 0.001$).

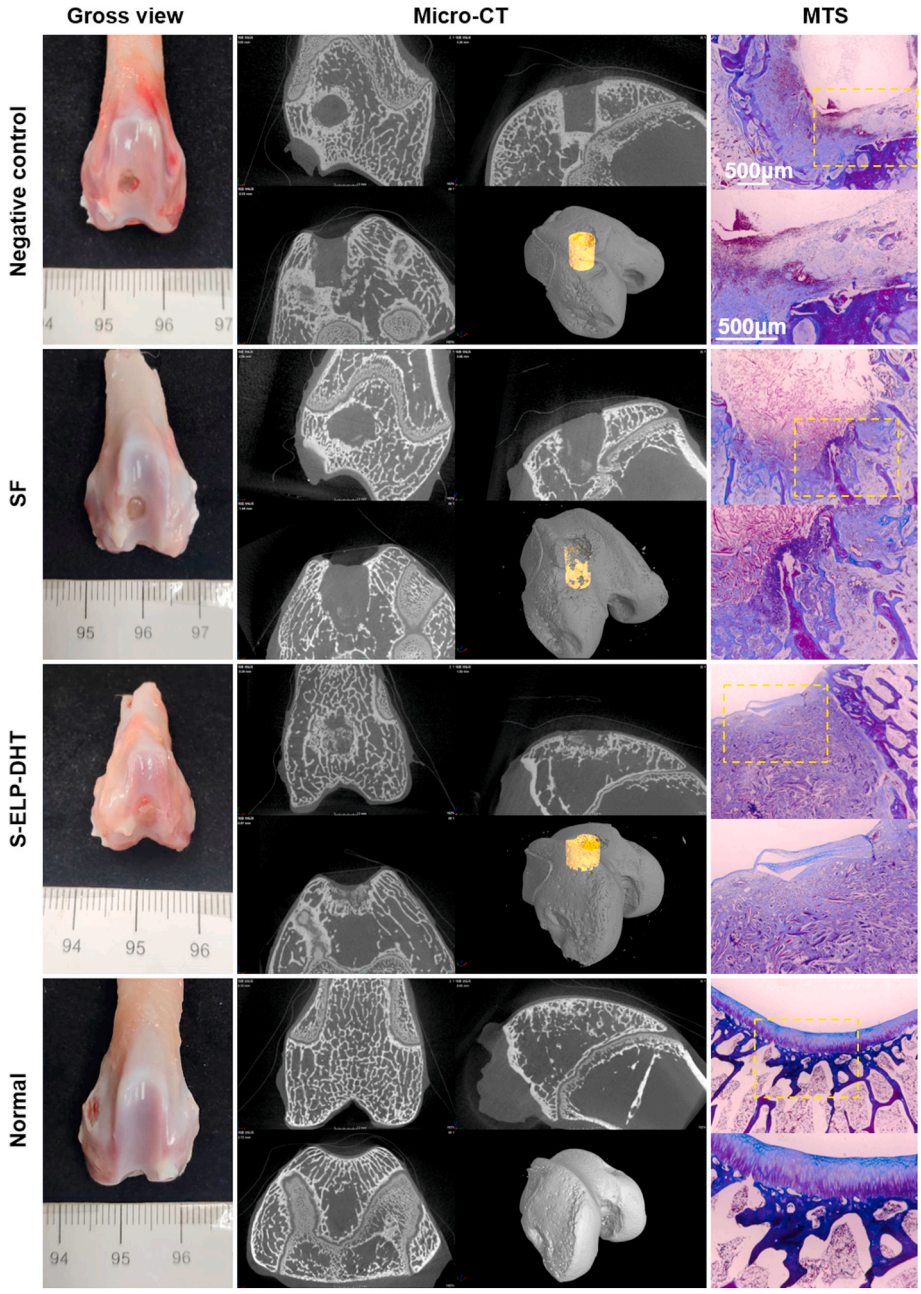

Fig. 9. Articular osteochondral repair in rabbits. Gross view, micro-CT analysis and MTS of representative cartilage joints from non-treated (negative control), SF and S-ELP-DHT groups at 2 months after implantation. Normal cartilage joint was used as a positive control. The yellow zones in MTS images were magnified and showed in the corresponding image underneath.

S-ELP-DHT scaffolds by implanting chondrocyte-seeded scaffolds into subcutaneous tissue of nude mice. After 1 and 2 months of implantation, both SF and S-ELP-DHT scaffolds formed white cartilage-like tissues (Fig. 7). As showed by the H&E staining, rudimental scaffold material was still visible without appearance of obvious inflammatory cells; additionally, the S-ELP-DHT scaffolds presented a higher density of compact cells and formed more cartilage lacunae (typical cartilage structures) as compared to SF scaffolds, especially at 1 month post-implantation (Fig. 7). Furthermore, S–O, TB and MTS staining confirmed the presence of large quantities of cartilage collagen and polysaccharides in the S-ELP-DHT scaffolds, indicating its superior ability to promote cartilage ECM formation *in vivo* (Fig. 7). We also performed immunofluorescence staining of Col II and Col X to evaluate the phenotype of the regenerated cartilage tissue (Fig. 7). As known, Col II (the key component of the cartilage matrix) is an indicator of articular cartilage, while Col X (secreted by hypertrophic chondrocytes during the endochondral bone formation) is a producer of calcifying cartilage [48,49]. According to the quantitative analysis of immunofluorescence staining results using Image J and SPSS software, there was no significant difference between Col II and Col X in each group. Notably, significantly higher amounts of Col II and Col X nodules were present and were well distributed in the S-ELP-DHT group at each time point. The above immunofluorescence staining results indicated that our S-ELP-DHT scaffolds could promote both articular and hypertrophic cartilage regeneration, demonstrating its potential for regeneration and remodelling of osteochondral defects.

To better interpret the regenerative outcomes of different groups, biomechanical and biochemical evaluations were carried out. As showed in Fig. 8A and Table S2, the compressive modulus of the regenerated tissues harvested at 2 months from the SF or S-ELP-DHT groups was significantly higher than their counterparts harvested at 1 month, implying that the prolonged *in vivo* implantation might help to generate more mature cartilaginous tissue. Notably, the S-ELP-DHT group after 2 months of implantation exhibited stronger compressive properties than SF group (43.24 ± 2.90 *vs.* 35.67 ± 2.81 MPa, $^{*}p < 0.05$) and native elastic cartilage (43.24 ± 2.90 *vs.* 14.97 ± 1.54 MPa, $^{***}p < 0.001$). Its compressive modulus was even comparable to that of normal fibrocartilage (43.24 ± 2.90 *vs.* 45.50 ± 2.20 MPa), enabling this scaffold to meet the mechanical requirements of functional articular cartilage. GAG quantification analysis further revealed that the S-ELP-DHT group had higher GAG contents than the SF group (21.70 ± 2.92 *vs.* 16.06 ± 1.50 mg/g, $^{**}p < 0.01$) after implantation *in vivo* for 2 months (Fig. 8B and Table S2). Although GAG content of the S-ELP-DHT group was lower than that of native elastic cartilage (21.70 ± 2.92 *vs.* 31.85 ± 3.13 mg/g, $^{***}p < 0.001$), its content was similar to that of native fibrocartilage (21.70 ± 2.92 vs. 21.56 ± 1.19 mg/g). Altogether, the above results indicated our S-ELP-DHT scaffolds could induce chondrocytes to produce more cartilage-specific matrix and significantly improve the level of cartilage formation (Fig. S7).

3.4. Assessments of articular cartilage and subchondral bone repair efficacy

Since our S-ELP-DHT scaffold was found able to enhance cell adhesion, infiltration and proliferation, promote the osteogenic differentiation of BMSCs and maintain the phenotype of chondrocytes *in vitro* and *in vivo*, we speculated that this scaffold could facilitate the repair of cartilage and subchondral bone. To evaluate its therapeutic efficacy for osteochondral regeneration, we implanted the scaffolds without cells into the rabbit articular osteochondral defects. After 2 months of implantation, from the gross view of the repaired cartilage tissues, defects in the negative control and SF groups were still clearly visible with little fibrillar tissue at the bottom of the drilling hole (Fig. 9). However, we found the regenerated tissues using the S-ELP-DHT group were well integrated with the surrounding cartilage tissues and exhibited white and smooth appearances closely resembling the normal cartilage (Fig. 9). Micro-CT and histological examination (MTS) additionally demonstrated that the osteochondral defects in the S-ELP-DHT scaffolds were repaired by more subchondral bone and thicker organized cartilage-like tissue than those in the negative control and SF groups (Fig. 9). Moreover, the neotissue was better integrated with the surrounding normal cartilage and subchondral tissue in the S-ELP-DHT group. These results indicated that the S-ELP-DHT scaffolds could enhance the new bone and neocartilage formation *in vivo*.

4. Conclusion

In the present study, we have developed a novel ELP-modified SF composite scaffold with porous fibrous structure and distinctive mechanical properties by a simple and green DHT treatment. Thanks to the facile and environment-friendly procedure and the high reproducibility, the scaffold preparation approach will be easy to popularize. Our S-ELP-DHT scaffold was found able to support the adhesion, proliferation and differentiation of BMSCs and/or chondrocytes *in vitro* and enhance the cartilage and subchondral bone repair *in vivo*. This scaffold combines the advantages of SF and ELP and offers a new solution for cartilage and osteochondral repair. Beyond osteochondral repair, we envision that our ELP modified SF scaffolds may also serve as a promising biomaterial to repair other tissues like skin.

CRediT authorship contribution statement

Zhuoyue Chen: Investigation, Methodology, Data curation, Formal analysis, Writing - original draft. **Qiang Zhang:** Methodology, Data curation, Writing - original draft. **Hongmin Li:** Validation, Writing - review & editing. **Qi Wei:** Validation, Writing - review & editing. **Xin Zhao:** Resources, Supervision, Project administration, Writing - review & editing. **Fulin Chen:** Resources, Supervision, Project administration, Funding acquisition, Writing - review & editing.

Declaration of competing interest

The authors declare that they have no known competing financial interests or personal relationships that could have appeared to influence the work reported in this paper.

Acknowledgments

This work was supported by the Departmental General Research Fund of the Hong Kong Polytechnic University (UAH2), the National Natural Science Foundation of P. R. China (No. 31670975, 21706212), Special Support Plan for High-level Talents, and Innovation Team Program in Shaanxi Province.

Appendix A. Supplementary data

Supplementary data to this article can be found online at https://doi.org/10.1016/j.bioactmat.2020.09.003.

References

[1] B.R. Mandelbaum, J.E. Browne, F. Fu, L. Micheli, J.B. Mosely, C. Erggelet, T. Minas, L. Peterson, Articular cartilage lesions of the knee, Am. J. Sports Med. 26 (6) (1998) 853–861.
[2] D.J. Huey, J.C. Hu, K.A. Athanasiou, Unlike bone, cartilage regeneration remains elusive, Science 338 (6109) (2012) 917–921.
[3] D. Zhu, H. Wang, P. Trinh, S.C. Heilshorn, F. Yang, Elastin-like protein-hyaluronic acid (ELP-HA) hydrogels with decoupled mechanical and biochemical cues for cartilage regeneration, Biomaterials 127 (2017) 132–140.
[4] Y. Yan, T. Sun, H. Zhang, X. Ji, Y. Sun, X. Zhao, L. Deng, J. Qi, W. Cui, H.A. Santos, H. Zhang, Euryale ferox seed-inspired superlubricated nanoparticles for treatment of osteoarthritis, Adv. Funct. Mater. 29 (4) (2019) 1807559.
[5] X. Ji, Y. Yan, T. Sun, Q. Zhang, Y. Wang, M. Zhang, H. Zhang, X. Zhao, Glucosamine sulphate-loaded distearoyl phosphocholine liposomes for osteoarthritis treatment: combination of sustained drug release and improved lubrication, Biomater Sci 7 (7) (2019) 2716–2728.

[6] Q. Yao, B. Wei, N. Liu, C. Li, Y. Guo, A.N. Shamie, J. Chen, C. Tang, C. Jin, Y. Xu, X. Bian, X. Zhang, L. Wang, Chondrogenic regeneration using bone marrow clots and a porous polycaprolactone-hydroxyapatite scaffold by three-dimensional printing, Tissue Eng. 21 (7–8) (2015) 1388–1397.
[7] M.J. Rodriguez, J. Brown, J. Giordano, S.J. Lin, F.G. Omenetto, D.L. Kaplan, Silk based bioinks for soft tissue reconstruction using 3-dimensional (3D) printing with in vitro and in vivo assessments, Biomaterials 117 (2017) 105–115.
[8] F. Zhou, X. Zhang, D. Cai, J. Li, Q. Mu, W. Zhang, S. Zhu, Y. Jiang, W. Shen, S. Zhang, H.W. Ouyang, Silk fibroin-chondroitin sulfate scaffold with immuno-inhibition property for articular cartilage repair, Acta Biomater. 63 (2017) 64–75.
[9] F. Mottaghitalab, H. Hosseinkhani, M.A. Shokrgozar, C. Mao, M. Yang, M. Farokhi, Silk as a potential candidate for bone tissue engineering, J. Contr. Release 215 (2015) 112–128.
[10] C. Guo, C. Li, H.V. Vu, P. Hanna, A. Lechtig, Y. Qiu, X. Mu, S. Ling, A. Nazarian, S.J. Lin, Thermoplastic moulding of regenerated silk, Nat. Mater. 19 (1) (2020) 102–108.
[11] X. Mu, V. Fitzpatrick, D.L. Kaplan, From silk spinning to 3D printing: polymer manufacturing using directed hierarchical molecular assembly, Adv. Healthc. Mater. (2020) 1901552.
[12] R.D. Abbott, E.P. Kimmerling, D.M. Cairns, D.L. Kaplan, Silk as a biomaterial to support long-term three-dimensional tissue cultures, ACS Appl. Mater. Interfaces 8 (34) (2016) 21861–21868.
[13] O. Hasturk, K.E. Jordan, J. Choi, D.L. Kaplan, Enzymatically crosslinked silk and silk-gelatin hydrogels with tunable gelation kinetics, mechanical properties and bioactivity for cell culture and encapsulation, Biomaterials 232 (2020) 119720.
[14] M. McGill, J.M. Grant, D.L. Kaplan, Enzyme-mediated conjugation of peptides to silk fibroin for facile hydrogel functionalization, Ann. Biomed. Eng. 48 (2020) 1905–1915.
[15] M. Rodriguez, J.A. Kluge, D. Smoot, M.A. Kluge, D.F. Schmidt, C.R. Paetsch, P.S. Kim, D.L. Kaplan, Fabricating mechanically improved silk-based vascular grafts by solution control of the gel-spinning process, Biomaterials 230 (2020) 119567.
[16] W. Shi, M. Sun, X. Hu, B. Ren, J. Cheng, C. Li, X. Duan, X. Fu, J. Zhang, H. Chen, Y. Ao, Structurally and functionally optimized silk-fibroin-gelatin scaffold using 3D printing to repair cartilage injury in vitro and in vivo, Adv. Mater. 29 (29) (2017) 1701089.
[17] B. An, T.M. DesRochers, G. Qin, X. Xia, G. Thiagarajan, B. Brodsky, D.L. Kaplan, The influence of specific binding of collagen-silk chimeras to silk biomaterials on hMSC behavior, Biomaterials 34 (2) (2013) 402–412.
[18] N. Sawatjui, T. Damrongrungruang, W. Leeanansaksiri, P. Jearanaikoon, S. Hongeng, T. Limpaiboon, Silk fibroin/gelatin–chondroitin sulfate–hyaluronic acid effectively enhances in vitro chondrogenesis of bone marrow mesenchymal stem cells, Mater. Sci. Eng. C 52 (2015) 90–96.
[19] J. Chen, G.H. Altman, V. Karageorgiou, R. Horan, A. Collette, V. Volloch, T. Colabro, D.L. Kaplan, Human bone marrow stromal cell and ligament fibroblast responses on RGD-modified silk fibers, J. Biomed. Mater. Res. A 67 (2) (2003) 559–570.
[20] L. Zheng, H.S. Fan, J. Sun, X.N. Chen, G. Wang, L. Zhang, Y.J. Fan, X.D. Zhang, Chondrogenic differentiation of mesenchymal stem cells induced by collagen-based hydrogel: an in vivo study, J. Biomed. Mater. Res. A 93 (2) (2010) 783–792.
[21] F. Zhou, X. Zhang, D. Cai, J. Li, Q. Mu, W. Zhang, S. Zhu, Y. Jiang, W. Shen, S. Zhang, Silk fibroin-chondroitin sulfate scaffold with immuno-inhibition property for articular cartilage repair, Acta Biomater. 63 (2017) 64–75.
[22] D.H. Le, A. Sugawara-Narutaki, Elastin-like polypeptides as building motifs toward designing functional nanobiomaterials, Mol. Syst. Des. Eng. 4 (3) (2019) 545–565.
[23] A.K. Varanko, J.C. Su, A. Chilkoti, Elastin-like polypeptides for biomedical applications, Annu. Rev. Biomed. Eng. 22 (2020) 343–369.
[24] S.M. Mithieux, A.S. Weiss, Design of an elastin-layered dermal regeneration template, Acta Biomater. 52 (2017) 33–40.
[25] J. Ozsvar, A. Tarakanova, R. Wang, M.J. Buehler, A.S. Weiss, Allysine modifications perturb tropoelastin structure and mobility on a local and global scale, Matrix Biol. 2 (2019) 100002.
[26] Q. Wen, S.M. Mithieux, A.S. Weiss, Elastin biomaterials in dermal repair, Trends Biotechnol. 38 (3) (2020) 280–291.
[27] D.L. Nettles, A. Chilkoti, L.A. Setton, Applications of elastin-like polypeptides in tissue engineering, Adv. Drug Deliv. Rev. 62 (15) (2010) 1479–1485.
[28] H. Betre, S.R. Ong, F. Guilak, A. Chilkoti, B. Fermor, L.A. Setton, Chondrocytic differentiation of human adipose-derived adult stem cells in elastin-like polypeptide, Biomaterials 27 (1) (2006) 91–99.
[29] B. Bavaresco, R. Comín, N.A. Salvatierra, M.P. Cid, Three-dimensional printing of collagen and hyaluronic acid scaffolds with dehydrothermal treatment crosslinking, Compos. Commun. 19 (2020) 1–5.
[30] B.B. Mandal, A. Grinberg, E.S. Gil, B. Panilaitis, D.L. Kaplan, High-strength silk protein scaffolds for bone repair, Proc. Natl. Acad. Sci. Unit. States Am. 109 (20) (2012) 7699–7704.
[31] X. Chen, L. Zhou, H. Xu, M. Yamamoto, M. Shinoda, M. Kishimoto, T. Tanaka, H. Yamane, Effect of the application of a dehydrothermal treatment on the structure and the mechanical properties of collagen film, Materials 13 (2) (2020) 377.
[32] Z. Luo, L. Jiang, Y. Xu, H. Li, W. Xu, S. Wu, Y. Wang, Z. Tang, Y. Lv, L. Yang, Mechano growth factor (MGF) and transforming growth factor (TGF)-β3 functionalized silk scaffolds enhance articular hyaline cartilage regeneration in rabbit model, Biomaterials 52 (2015) 463–475.
[33] Z. Chen, Y. Song, J. Zhang, W. Liu, J. Cui, H. Li, F. Chen, Laminated electrospun nHA/PHB-composite scaffolds mimicking bone extracellular matrix for bone tissue engineering, Mater. Sci. Eng. C 72 (2017) 341–351.
[34] Z. Chen, J. Wei, J. Zhu, W. Liu, J. Cui, H. Li, F. Chen, Chm-1 gene-modified bone marrow mesenchymal stem cells maintain the chondrogenic phenotype of tissue-engineered cartilage, Stem Cell Res. Ther. 7 (1) (2016) 70–81.
[35] R. Zheng, H. Duan, J. Xue, Y. Liu, B. Feng, S. Zhao, Y. Zhu, Y. Liu, A. He, W. Zhang, The influence of Gelatin/PCL ratio and 3-D construct shape of electrospun membranes on cartilage regeneration, Biomaterials 35 (1) (2014) 152–164.
[36] X. Zhao, I. Olsen, H. Li, K. Gellynck, P.G. Buxton, J.C. Knowles, V. Salih, A.M. Young, Reactive calcium-phosphate-containing poly (ester-co-ether) methacrylate bone adhesives: chemical, mechanical and biological considerations, Acta Biomater. 6 (3) (2010) 845–855.
[37] Z. Chen, Z. Zhang, J. Feng, Y. Guo, Y. Yu, J. Cui, H. Li, L. Shang, Influence of mussel-derived bioactive BMP-2-decorated PLA on MSC behavior in vitro and verification with osteogenicity at ectopic sites in vivo, ACS Appl. Mater. Interfaces 10 (14) (2018) 11961–11971.
[38] S. Gomes, G. Rodrigues, G. Martins, C. Henriques, J. Silva, In vitro evaluation of crosslinked electrospun fish gelatin scaffolds, Mater. Sci. Eng. C 33 (3) (2013) 1219–1227.
[39] Y.N. Zhang, R.K. Avery, Q. Vallmajo-Martin, A. Assmann, A. Vegh, A. Memic, B.D. Olsen, N. Annabi, A. Khademhosseini, A highly elastic and rapidly crosslinkable elastin-like polypeptide-based hydrogel for biomedical applications, Adv. Funct. Mater. 25 (30) (2015) 4814–4826.
[40] D.W. Lim, D.L. Nettles, L.A. Setton, A. Chilkoti, In situ cross-linking of elastin-like polypeptide block copolymers for tissue repair, Biomacromolecules 9 (1) (2008) 222–230.
[41] J. Yeo, W. Huang, A. Tarakanova, Y.W. Zhang, D.L. Kaplan, M.J. Buehler, Unraveling the molecular mechanisms of thermo-responsive properties of silk-elastin-like proteins by integrating multiscale modeling and experiment, J. Mater. Chem. B 6 (22) (2018) 3727–3734.
[42] R.N. Parker, D.M. Cairns, W.A. Wu, K. Jordan, C. Guo, W. Huang, Z. Martin-Moldes, D.L. Kaplan, Smart material hydrogel transfer devices fabricated with stimuli-responsive silk-elastin-like proteins, Adv. Healthc. Mater. 9 (11) (2020) 2000266.
[43] A.J. Engler, S. Sen, H.L. Sweeney, D.E. Discher, Matrix elasticity directs stem cell lineage specification, Cell 126 (4) (2006) 677–689.
[44] J. Wu, L. Cao, Y. Liu, A. Zheng, D. Jiao, D. Zeng, X. Wang, D.L. Kaplan, X. Jiang, Functionalization of silk fibroin electrospun scaffolds via BMSC affinity peptide grafting through oxidative self-polymerization of dopamine for bone regeneration, ACS Appl. Mater. Interfaces 11 (9) (2019) 8878–8895.
[45] Y. Yang, H. Lin, H. Shen, B. Wang, G. Lei, R.S. Tuan, Mesenchymal stem cell-derived extracellular matrix enhances chondrogenic phenotype of and cartilage formation by encapsulated chondrocytes in vitro and in vivo, Acta Biomater. 69 (2018) 71–82.
[46] Y.P. Singh, M. Adhikary, N. Bhardwaj, B.K. Bhunia, B.B. Mandal, Silk fiber reinforcement modulates in vitro chondrogenesis in 3D composite scaffolds, Biomed. Mater. 12 (4) (2017) 045012.
[47] D.L. Nettles, K. Kitaoka, N.A. Hanson, C.M. Flahiff, B.A. Mata, E.W. Hsu, A. Chilkoti, L.A. Setton, In situ crosslinking elastin-like polypeptide gels for application to articular cartilage repair in a goat osteochondral defect model, Tissue Eng. 14 (7) (2008) 1133–1140.
[48] H. Rogan, F. Ilagan, X. Tong, C.R. Chu, F. Yang, Microribbon-hydrogel composite scaffold accelerates cartilage regeneration in vivo with enhanced mechanical properties using mixed stem cells and chondrocytes, Biomaterials 228 (2020) 119579.
[49] D. Lin, B. Cai, L. Wang, L. Cai, Z. Wang, J. Xie, Q. Lv, Y. Yuan, C. Liu, S.G. Shen, A viscoelastic PEGylated poly (glycerol sebacate)-based bilayer scaffold for cartilage regeneration in full-thickness osteochondral defect, Biomaterials 253 (2020) 120095.